Title: Bacterial filamentation is an in vivo mechanism for cell-to-cell spreading

Authors: Tuan D Tran[1], Munira Aman Ali[1], Davin Lee[1], Marie-Anne Félix[2], Robert J Luallen[1*]

Affiliations:

[1]Department of Biology, San Diego State University, San Diego, CA 92182, USA

[2]Institut de Biologie de l' École Normale Supérieure, Centre National de la Recherche Scientifique, INSERM, École Normale Supérieure, Paris Sciences et Lettres, Paris, France

[*]Corresponding author. Email: rluallen@sdsu.edu

ABSTRACT

Intracellular pathogens are challenged with limited space and resources while replicating in a single host cell. Mechanisms for direct invasion of neighboring host cells have been discovered in cell culture, but we lack an understanding of how bacteria directly spread from cell-to-cell in vivo. Here, we describe the discovery of a bacterial species that uses filamentation as an in vivo mechanism for intracellular spreading between the intestinal epithelial cells of its host, the rhabditid nematode *Oscheius tipulae*. In vitro and in vivo filamentation by this bacterium, *Bordetella atropi*, requires a highly conserved nutrient-sensing pathway used by divergent bacteria to detect rich conditions and inhibit the divisome. Thus, *B. atropi* uses a distinct mechanism for cell-to-cell spreading by coopting a pathway that normally regulates bacterial cell size to trigger filamentation inside host cells.

INTRODUCTION

Pathogenic invasion of host cells often provides microbes with a major benefit, including a high concentration of metabolic resources and protection from extracellular immunity[1]. An individual host cell, however, represents a small niche and it is advantageous for intracellular pathogens to spread to other cells in order to maximize the use of host resources. All intracellular microbes can spread via extracellular escape from the initial infected cell, a process that leaves them vulnerable to host defenses. Some microbes, however, have evolved unique mechanisms to invade uninfected host cells directly from an initial infected cell. To date, two main paradigms for cell-to-cell spreading by bacteria have been described, both of which converge on effector-driven manipulation of host actin. In one mechanism, *Listeria monocytogenes*, *Shigella flexneri*, and *Rickettsia spp.* can polymerize host actin for cytoplasmic propulsion of bacteria into the lateral membrane for uptake by neighboring cells[2]. *Burkholderia* spp. also use actin-based propulsion, but invasion of neighboring cells is facilitated by fusion of the lateral membranes[3]. In another mechanism, *Ehrlichia chaffeensis* can directly transfer from a phagocytic cell to a target cell through actin-dependent filopodia formation, although it is unclear if this mechanism is directly initiated by the pathogen[1,4]. Each of these bacterial mechanisms has only been directly observed in cell culture systems, bringing up the possibility of alternative mechanisms for cell-to-cell spreading and dissemination in vivo[5].

Bacteria often change their cell shape as a fitness strategy to survive or thrive in diverse environments. Filamentation is an example of this morphological plasticity, often used as a survival strategy in toxic or stressful environments. During filamentation, there is a dramatic increase in cell length as a bacterium divides longitudinally multiple times without daughter cell separation, often without septation[6,7]. Gram-negative bacteria are mainly known to undergo filamentation after exposure to environmental stressors, including DNA damage and β-lactam antibiotics, which induce the SOS response[6]. Several bacterial pathogens, such as *H. influenzae*, *P. aeruginosa*, *Y. pestis*, have been observed to filament in vivo, including inside host cells[8]. However, to our knowledge, filamentation has never been observed to be used for cell-to-cell spreading by any intracellular pathogen, including bacteria or fungi[9]. In this work, we describe the discovery of an intracellular bacterial pathogen that uses filamentation to directly spread from cell to cell in the

intestine of an animal host. Initiation of intracellular filamentation by this pathogen requires a highly conserved metabolic pathway used by divergent bacteria to detect rich conditions to delay divisome assembly.

RESULTS

Discovery and characterization of *Bordetella atropi*

Wild-caught nematodes and their naturally associated pathogens have served as models to dissect different aspects of host-microbe interactions[10–12]. Given their transparency, these nematodes allow for the visualization and dissection of novel aspects of microbial pathogenesis and host immune/stress responses[13–15]. Known natural intracellular pathogens infecting free-living nematodes include viruses and microsporidia, but prior to now, no intracellular bacteria have been identified[16]. From ecological sampling, we isolated a wild *Oscheius tipulae* strain (JU1501) from rotting crab apples (Supplementary Fig. 1). *O. tipulae* is a rhabditid species that is commonly found in soil and decomposing vegetation[17]. In JU1501, coccobacilli-shaped microbes were observed to infect the intestinal epithelial cells (Fig. 1a). Since microsporidian parasites are the most common intracellular pathogens found in wild *C. elegans* and other free-living nematodes[18,19], this microbe was originally reported in a large survey of microsporidia based on morphology, despite the failure of microsporidian-specific 18S primers to produce an amplicon[19]. We conducted fluorescence in situ hybridization (FISH) on mixed-stage populations of this *O. tipulae* strain and found that a mixture of microsporidian-specific 18S probes failed to bind (Supplementary Fig. 2a). Given the lack of hybridization of this microbe to commonly infecting microsporidian species associated with wild nematodes, we suspected it may instead be a bacterium. Indeed, a universal probe to bacterial 16S rRNA showed strong hybridization with a multitude of coccobacilli inside the animals (Fig. 1b). In addition to these coccobacilli, we also observed a second bacterial morphology in some animals in the same sample in which long filaments extended throughout the intestine (Fig. 1c). Identical phenotypes were seen using a FISH probe specific to the 16S rRNA of this filamenting coccobacillus bacterium but not a non-specific bacterial 16S probe (Supplementary Fig. 2b-c).

We isolated this bacterium on LB agar plates (strain name LUAb4) and verified that it could reinfect JU1501 *O. tipulae* animals that were sterilized of all horizontally-transmitted microbes using a bleach treatment (as seen Fig. 1e-g). We sequenced the genome of LUAb4 and conducted phylogenomic analysis to find that the bacterium represents a new species in a separate monophyletic clade of *Bordetella* (Fig. 1d), clustering with Bordetellae isolated from human respiratory specimens or the environment. We named this bacterium *Bordetella atropi*, after Atropos, the Greek Fate who cuts the thread of life (Supp. Text 1, Taxonomic Summary). Similar to other Bordetellae, *B. atropi* has the appearance of a coccobacillus morphology when in its non-filamentous form[20]. Infection by *B. atropi* has a severe effect on host fitness with an approximate 2.5-fold decrease in average lifespan and 90-fold decrease in fecundity (Fig. 1e-f). To determine the order of appearance of *B. atropi* phenotypes in vivo, we conducted a pulse-chase infection experiment and found that the most animals had a majority of bacteria displaying either short or long intracellular filaments at 16 and 24 hours post infection (hpi), while most animals had

a majority of bacteria in the coccobacilli form at 38 and 48 hpi (Fig. 1g). When we used confocal microscopy on FISH-stained animals at 34 hours post infection (hpi), we found that the average in vivo filament length of WT *B. atropi* was 51.9 μm with a maximum of 130 μm, or approximately 130 bacterial cell lengths (Fig. 1h).

Bordetella atropi **is an intestinal intracellular pathogen**

Our observations of *B. atropi* infection by light microscopy suggested that coccobacilli were predominantly inside intestinal epithelial cells (Fig. 1a). To verify the intracellular nature and tissue tropism of *B. atropi*, we conducted transmission electron microscopy (TEM) of infected animals at 24 and 48 hpi. The intestine of *O. tipulae* is comprised of pairs of tubulating epithelial cells along the anterior-posterior axis, except at the most anterior portion of the intestine where four epithelial cells surround the lumen[21]. This intestine is separated from the body wall muscle, epidermis, and germline by a narrow space that forms the pseudocoelom (Fig. 2a). In uninfected animals, the intestinal cells can be distinguished by a relatively lighter electron density than other tissues, the presence of the intestinal lumen with microvilli, and a uniform distribution of intracellular gut granules (Fig. 2b). *B. atropi* coccobacilli and filaments were distinguished from host cellular structures by a wavy, electron dense cell wall surrounding large, electron poor nucleoids, similar to TEM images of intracellular *Bordetella bronchiseptica*[22], and these phenotypes were not observed in uninfected animals (Fig. 2c-e). At 24 hpi, we can see filaments with this characteristic cell wall delineation in intestinal cells that are unseptated with regularly spaced nucleoids and coccobacilli in the intestinal lumen (Fig. 2f-g). TEM only captures a portion of a filament length due to thin sectioning and the longest filament captured with this method was 10.06 μm (Fig. 2f), as compared to the average filament length of 51.86 μm as determined by tracing individual distinguishable filaments by confocal microscopy (see Fig. 1h). Of note, we also observed instances where nucleoids appear to be dividing and potential septum formation in these filaments (Fig. 2g). By 48 hpi, we see intestinal cells that are heavily infected with individual coccobacilli cells (Fig. 2h). Notably, in cases where we could see lumenal bacteria at both 24 hpi and 48 hpi time points, the lumenal coccobacilli bear the same morphological characteristics of those detected in the intracellular environment (see Fig. 2c, lower right for lumenal coccobacilli). Using quantification, we found that 42% of images displayed intestinal filaments at 24 hpi (n=52), and only 6.5% at 48 hpi (n=31), showing a similar trend to the emergence of phenotypes in vivo via fluorescence microscopy (see Fig. 1g). Separately, TEM bolstered the intestinal tropism seen with *B. atropi* as 70.6% of images had intracellular intestinal infection (n=102), but no infection was seen in non-intestinal tissues, including the muscle (n=38) and epidermis (n=73). The lateral intestinal membranes appear disrupted in infected animals as they are often missing or at oblique angles relative to the intestinal lumen in infected cells. This is in contrast to uninfected cells where they are relatively perpendicular to the lumen (Supplementary Fig. 3). While the use of electron dense delineation cannot unambiguously identify *B. atropi*, their absence in uninfected animals, the morphological similarities between those seen in intestinal cells and the lumen, as well as their high abundance at 48 hpi (similar to the FISH time course) indicate that these structures are characteristic of *B. atropi*. Together, these observations suggest that *B. atropi* is an intracellular pathogen that first

filaments in intestinal epithelial cells and later septates into individual coccobacilli before exiting the host cell.

As a parallel approach to TEM, we also employed fluorescent dyes that mark the intracellular environment of intestinal cells and confocal microscopy to investigate the localization of *B. atropi* in infected animals. Using CFSE, which strongly stains the cytoplasm of intestinal cells, we could observe the localization of *B. atropi* only within the boundary of the intestinal cell cytoplasm through z-stacks and orthogonal projections (Fig. 3a-b). Notably, we observed areas of CFSE-fluorescence clearing that overlap with the red fluorescence of *B. atropi* 16S probe (Fig. 3c, arrowheads in CFSE channel). This loss of CFSE fluorescence in these areas are likely due to bacterial filaments occupying these spaces, strongly supporting the cytoplasmic localization of *B. atropi* filaments (Fig. 3c).

Additionally, we used fluorophore-tagged phalloidin to stain host actin filaments, including apical ACT-5 and cortical actin filaments at the basolateral side of the intestine (Fig. 3d-e). In cases where phalloidin staining clearly showed the apical and basolateral perimeters of intestinal cells, we observed that *B. atropi* filaments and coccobacilli were localized within this actin staining. A representative line profile analysis shows that RFP-tagged bacteria lie in between positions of basal and apical actin filaments in the intestine and close to nucleus, suggesting that *B. atropi* localizes within intestinal cells (Fig. 3f). We quantitated these images and found that 92.5% of infection events (i.e., coccobacilli or filaments) stay well within the boundaries of intestinal actin filaments, whereas 7.5% of infection events were ambiguous in their localization as there was direct overlap with the basal actin filament and we could not clearly assign localization to them (Fig. 3g). However, we did not observe any infection events that were clearly extracellular, where bacterial phenotypes appeared beyond the basal actin filament boundary of intestinal cells (0% extracellular) nor did we observe bacteria colocalizing with the body wall muscle. Separately, with phalloidin straining we also observed instances where bacterial filaments were pushing through the lateral actin filaments of intestinal cells, suggesting that these filaments were crossing through the cell-cell boundary between intestinal cells, reminiscent of the TEM result (Fig. 3h-i). Altogether, these data strongly support the intracellular nature and intestinal tropism of *B. atropi*.

Filamentation by *B. atropi* is used for cell-to-cell spreading

We hypothesized that filamentation by *B. atropi* is used as a mechanism for cell-to-cell spreading. Often, we observed cases where filaments passed near multiple intestinal nuclei, indicating that the bacterium was simultaneously infecting neighboring intestinal cells (Fig. 4a). To test this hypothesis, we sought to isolate a non-filamenting mutant of *B. atropi*. Similar to *Bordetella avium*[23], our bacterium could be induced to filament in vitro by switching growth from Luria broth (LB) to the richer medium Terrific broth (TB) (Supplementary Fig. 4a), allowing us to use in vitro selection to isolate filamentation mutants (Fig. 4b). We focused on one mutant, LUAb7, which formed less frequent and much shorter filaments in vitro compared to wild type (Fig. 4c) but grew at the same rate (Fig. 4d). In vivo infection of *O. tipulae* found that LUAb7 also showed significantly decreased anterior-posterior spreading (Supplementary Fig. 4b-c). We confirmed that LUAb7 still infects the cytoplasm of intestinal cells in vivo using the cytoplasmic dye CFSE (Supplementary Fig. 5a-b).

Further in vivo characterization of LUAb7 showed that the main phenotype of the bacteria in infected animals is coccobacilli throughout the course of infection, with areas filled with coccobacilli increasing as the infection progresses (Supplementary Fig. 5c-d). LUAb7 also forms much shorter filaments compared to WT, with an average length of 6.55 μm (Supplementary Fig. 5e), and even though LUAb7 failed to form long filaments in vivo, it still sufficiently reduced host genetic fitness to the same level as WT, suggesting that other virulence mechanisms may affect host fitness (Supplementary Fig. 5f-g).

The intestine of *O. tipulae* consists of left-right pairs of polarized epithelial cells running along the anterior-posterior (A-P) axis[21] (Fig. 2a). To quantify the cell-to-cell spreading capacity of WT and LUAb7, we pulse infected animals for a short period to limit the number of invasion events and then counted the number of intestinal nuclei that each contiguous infection event passes along the A-P axis. A contiguous infection event is assumed to be the result of replication from a single bacterium. For distinguishable filaments, we assume each filament is the replicative product from a single invasion event. However, we also observed infection foci, especially with LUAb7 infection. These foci are tightly packed clusters of coccobacilli, or a mixture of closely spaced short filaments (4-8 μm) and coccobacilli, and each focus is well separated from each other (Supplementary Fig. 6). We assume one infection focus is the result of one infection event in which the original invading bacterium underwent normal binary division, however, it is also possible that an infection focus is the result of more than one infection event. We observed both phenotypes in animals infected with either WT or LUAb7 strain, albeit at markedly different frequencies. For the WT strain, 95% of infection events were filaments and 5% were foci (n=162), whereas 9% of infection events were distinguishable filaments (8-14 μm) and 91% were foci (n=131) in case of LUAb7. When we followed single WT *B. atropi* filaments in vivo, they spanned an average of 5.7 and a maximum of 15 intestinal nuclei (Fig. 4e-f). By contrast, LUAb7 failed to consistently form filaments in vivo, with replicating infection foci seen spanning an average of 1.9 and a maximum of 4 intestinal nuclei. Similar to *C. elegans,* intestinal nuclei in *O. tipulae* may undergo one nuclear division without cell division during development. Using intestinal membrane staining, we quantified an average of 1.9 intestinal nuclei per cell at both the anterior and posterior end (Supplementary Fig. 7). Therefore, WT *B. atropi* filaments spread laterally to an average of 3 cells and a maximum of 8 cells at 34 hpi, while the filamentation mutant remains largely restricted to a single cell but occasionally spreads to another cell. Altogether, these data indicate that *B. atropi* uses filamentation as an intracellular mechanism for cell-to-cell spreading.

A conserved metabolic pathway controls *B. atropi* filamentation

We identified the causative mutation in LUAb7 through whole genome sequencing and single nucleotide variations (SNVs) calling. The best candidate was a missense mutation found in *gtaB*, a UTP--glucose-1-phosphate uridylyltransferase. The mutation in *gtaB* lead to an R17C change in a predicted catalytic arginine found in a highly conserved N-terminal motif (Fig. 5a)[24]. We complemented LUAb7 with $gtaB^{+}$ from *B. atropi* and found a rescue of in vitro filamentation (Fig. 5b) as well as in vivo filamentation, with similar levels of cell-to-cell spreading as wild type (Fig. 4e-f). Additionally, deletion of *gtaB* from WT *B. atropi* resulted in a loss of filamentation in vitro, similar to $gtaB^{R17C}$ (Fig. 5d). Thus, $gtaB^{R17C}$ is the causative allele for loss of

filamentation in LUAb7 and this single mutation abolishes cell-to-cell spreading of the pathogen.

GtaB (GalU in *E. coli*) catalyzes the conversion of glucose-1-phosphate to UDP-glucose, a substrate in the production of cell wall components like osmoregulated periplasmic glucans (OPGs), lipopolysaccharide, and capsular polysaccharides (Fig. 4c). In *E. coli* and *Bacillus subtilis*, this UDP-glucose biosynthetic pathway serves as a metabolic sensor that links carbon availability to growth rate[25]. Excess UDP-glucose acts as a readout for rich conditions and temporarily inhibits FtsZ ring formation during replication for moderately larger progeny cells[26,27]. In *E. coli,* FtsZ ring inhibition is mediated by OpgH, a downstream glucosyltransferase that is thought to sequester FtsZ monomers at the nascent division site in a UDP-glucose-dependent manner (Fig. 5c)[26]. We tested other members in this pathway for a role in filamentation by knocking them out in *B. atropi*. Deletion of *opgH* resulted in a loss of filamentation in vitro, similar to LUAb7(*gtaB*^{R17C}) (Fig. 5d). The *B. atropi* genomes contained two copies of phosphoglucomutase (pgm) and deletion of *pgm2* but not *pgm1* resulted in loss of in vitro filamentation (Fig. 5d). Surprisingly, knockout of *pgm1* did not phenocopy LUAb7 but instead led to an increase in in vitro filamentation. This finding suggests that *pgm1* may negatively regulate UDP-glucose biosynthesis, as a similar role has been suggested for *galF* in *E. coli*, which may antagonize *galU* in the same pathway[28].

We then tested these knockouts in vivo. The *opgH* knockout phenocopied LUAb7(*gtaB*^{R17C}), with reduced A-P spreading in the intestine (Fig. 5e). We verified that this decreased A-P spreading was not due to decreased infectivity, as LUAb7 (*gtaB*^{R17C}), *ΔgtaB*, and *Δpgm1* all had similar initial invasion events as WT at 16 hpi under our pulse-chase infection procedure (Supplementary Fig. 8). By contrast, the *pgm1* knockout showed no change in spreading in vivo compared to WT, consistent with in vitro data. While both the *Δpgm2* and *ΔgtaB* strains showed an inability to filament in vitro, we found that they were attenuated in vivo, as we saw no intracellular infection with these strains despite populations of >500 animals per replicate (Supplementary Fig. 9). In fact, we saw little to no bacteria in the intestinal lumen with these knockouts, suggesting that a complete loss of some cell wall components may result in an inability to survive feeding by *O. tipulae*, perhaps leaving bacteria sensitive to the posterior grinder and/or destruction by extracellular defenses in the lumen. Altogether, these results support a requirement for the UDP-glucose biosynthetic pathway and *opgH* in inhibiting cell fission in *B. atropi*, but in a more extreme manner than seen in *E. coli* and *B. subtilis,* leading to long multinucleoid filaments rather than bacilli with modestly increased lengths. Overall, we propose a model where *B. atropi* detects the nutrient-rich intracellular environment of an intestinal cell through the UDP-glucose biosynthetic pathway and OpgH in order to initiate filamentation for cell-to-cell spreading (Fig. 5f).

DISCUSSION

Together, our findings describe bacterial filamentation as an in vivo mechanism for cell-to-cell spreading in a host epithelium. Several human-infecting bacterial pathogens have been observed to filament in vivo, including some that filament intracellularly, bringing up the possibility that some pathogens may use filamentation as a spreading mechanism[7,8]. Uropathogenic *E. coli* (UPEC) can form extremely

long filaments inside umbrella cells, with conflicting data on whether these filaments are refractory to phagocytosis by macrophages after their release from host cells[29,30]. Intracellular bacterial filaments can distort host cell shape in cell culture, as *Yersinia pestis* filaments in macrophages can make protrusions in the host cell membrane[31] and *Salmonella typhimurium* filaments can grossly distort and elongate primary melanocytes[32]. We observed similar phenotype in B. atropi whereby bacterial filaments push against and distort the lateral actin filaments of host intestinal cells. It is possible that exaggerated longitudinal growth is an in vivo strategy that intracellular pathogens can use to push through the lateral membranes in an epithelial layer for invasion of neighboring cells. For example, microsporidian parasites in *C. elegans* can form elongated intracellular stages (called meronts) that distort lateral intestinal membranes, leading to the formation of a syncytial tissue and cell-cell spreading[13].

We found that filamentation induction by *B. atropi* is linked to nutrient availability through a highly conserved metabolic pathway that inhibits the bacterial divisome under rich conditions. These findings represent a new mechanism for the induction of filamentation in bacteria that is independent of the SOS response. Given the broad conservation of the UDP-glucose pathway and its role in delaying binary division on rich media[26,27], it is possible that the evolutionary steps for coopting this pathway for filamentation are minimal. For example, experimental overexpression of *opgH* in *E. coli* is sufficient to lead to filamentation, showing that altering the expression of a single gene in the pathway can induce this phenotype[26]. *B. avium* is a respiratory pathogen of turkeys and was found to form filaments in TB similar to *B. atropi*, bringing up the possibility that filamentation in rich conditions is conserved among other clinically-relevant Bordetellae[23].

METHODS

Nematode and bacterial strains

Wild *O. tipulae* strain JU1501 was isolated from a rotting apple from Kerarmel, Plouezoc'h, France (GPS coordinates 48.65151, -3.85573) on August 6, 2008. *B. atropi* type strain LUAb4 was isolated from JU1501 through cleaning of dauer animals to remove contaminating microbes in M9 buffer + 0.25% SDS, 50 ug/mL of carbenicillin, 25 ug/mL of kanamycin, 12.5 ug/mL of tetracyclin, 100ug/mL of gentamycin, 50 ug/mL of streptomycin, 37.5 ug/mL of chloramphenicol, and 200 ug/mL of cefotaxime[33]. After cleaning of JU1501, non-OP50-1 colonies were seen growing on nematode growth media (NGM) plates containing this strain. Single colonies were streaked to LB plates twice to ensure purity and the 16S rDNA was sequenced using primers 27F (AGAGTTTGATCMTGGCTCAG) and 1492R (GGTTACCTTGTTACGACTT).

Fluorescent in situ hybridization (FISH)

FISH was performed as described previously[34]. Probes to the small subunit rRNA of bacteria and microsporidia were conjugated to either CAL Fluor Red 610 (CF610) or 5-Carboxyfluorescein (FAM). The probes used were MicroA-CF610 (CTCTG TCCATCCTCGGCAA), MicroC-CF610 (CAGAATCAACCTGGTGCCTT), and MicroE-CF610 (GTACTGGAAATTCCGTGTTC), *B. atropi*-specific 16S probe b004 (TTATCCAGCGCCGTTTCTTTC), EUB338 (GCTGCCTCCCGTAGGAGT), and Alphaproteobacteria-specific 16S b002 (TGTACCGACCCTTAACGTTC).

Fitness assays

Lifespan assays were with conducted using a bleached strain of JU1501 to remove all horizontally transmitted microbes. Assays were conducted in technical triplicate across two separate trials with n=20 animals per plate seeded with either OP50-1 (the standard *E. coli* food source) or LUAb4 (*B. atropi*). Plates were grown at 23°C and animals were scored every 24 hours for death by touching non-motile animals with a pick. Accidentally killed and missing animals were censored from the count, but animals killed due to bagging were counted due to the possibility of infection-induced bagging. Brood size assays were conducted similarly, except n=20 animals per condition were plated to individual plates across two separate trials. The number of viable (hatched) progeny were counted every 24 hours and removed from the plate.

Standard pulse infection procedure

Two days prior to the infection, NGM plates were fully covered with 1 mL of an overnight culture of *B. atropi* strains or OP50-1 (OD_{600} ~ 0.4-0.5) and bacteria were allowed to grow into a full lawn at room temperature. On the day of infection, animals JU1501 grown on standard OP50-1 food source were collected with M9T buffer (M9 buffer, 0.05% TritonX-100), transferred onto *B. atropi* plates, and incubated 2 hrs at 23°C to allow infection to occur. Then, animals were washed off plates into 15 mL centrifuge tubes, washed 4 times with M9T for 20 minutes, and plated onto the OP50-1 plates. Animals are incubated at 23°C for indicated hours then processed by different assays and techniques as described below.

Pulse-chase infection time course

JU1501 animals were infected using the standard pulse infection procedure (see above). Animals were harvested at 16, 24, 36, and 48 hpi and FISH was performed as above with the *B. atropi* b004 probe. Images were taken and blinded for analysis, with animals binned as short filaments, long filaments, or filled with coccobacilli based on the majority phenotype seen in the animal. Uninfected animals or those with solely dispersed coccobacilli (representing recent invasion) were not counted. Samples were then unblinded and the percent of each phenotype at each timepoint was calculated separately for each replicate.

Transmission electron microscopy (TEM)

Animals were grown on OP50-1 to mixed stages were infected with wild-type *B. atropi* with the standard pulse infection procedure. At 24, 36, and 48 hours post infection, animals were harvested with M9 buffer, washed thoroughly with M9 for a couple times until the washing buffer looked sufficiently clear. Animals were then fixed with FGC fixative (2% paraformaldehyde, 2.5% glutaraldehyde in 0.1M cacodylate buffer pH 7.4) for 2 hours at room temperature on a rotator. Fixed samples were then kept in the same fixative at 4°C until further processing for TEM. TEM was performed by the Electron Microscopy Facility, Department of Cellular and Molecular Medicine at UCSD as described previously[34].

Genome sequencing and assembly

B. atropi strain LUAb4 was cultured from a single colony in LB and DNA was purified using the DNeasy Blood and Tissue Kit (Qiagen). Libraries were made using Illumina Nextera DNA Library from ~700 bp fragments and sequenced on Illumina MiSeq 2x250 bp by GeneWiz Inc. Unprocessed reads were assembled with SPAdes (v3.13.0) using the 'careful' parameter and testing 21, 33, 55, 77, 99, and 127 kmers[35]. Annotation was conducted with prokka (v1.14.0) with the parameters 'addgenes' 'genus Bordetella', and an evalue of 1e-06[36]. This Whole Genome Shotgun project has been deposited at DDBJ/ENA/GenBank under the accession JAHPZX000000000. The version described in this paper is version JAHPZX010000000.

Phylogenomics analyses

Phylogenomics was conducted using the UBGC pipeline as described[37], using 92 up-to-date bacterial core genes isolated from *B. atropi* and the following sequenced genomes: RHXM01000001.1 (*A. aegrifaciens*), UFQB01000001.1 (*A. agilis*), PYAL01000001.1 (*A. aloeverae*), AGUF01000105.1 (*A. arsenitoxydans*), CP013923.1 (*A. denitrificans*), VBUB01000010.1 (*A. dolens*), CP019325.1 (*A. insolitus*), GL982451.1 (*A. insuavis*), NJIG01000010.1 (*A. marplatensis*), QAYS01000001.1 (*A. mucicolens*), BCTK01000001.1 (*A. piechaudii*), CP017433.1 (*A. ruhlandii*), LGVG01000001.1 (*A. spanius*), LN831029.1 (*A. xylosoxidans*), CP013119.1 (*Alcaligenes faecalis*), FKIF01000001.1 (*B. ansorpii*), NC_010645.1 (*B. avium*), CP016170.1 (*B. bronchialis*), NC_019382.1 (*B. bronchiseptica*), CP016172.1 (*B. flabilis*), NEVR01000007.1 (*B. genomosp. 1*), NZ_CP012076.1 (*B. hinzii*), NZ_CP007494.1 (*B. holmesii*), NC_018828.1 (*B. parapertussis*), NC_002929.2 (*B. pertussis*), NC_010170.1 (*B. petrii*), NZ_CP016440.1 (*B. pesudohinzii*), and NZ_LT546645.1 (*B. trematum*). Alignments were made with RAxML based on amino acid sequences. Trees were made in MEGA X using maximum likelihood with 500 bootstraps using AA substitution via JTT model and tree inference using Nearest-Neighbor-Interchange.

Bacterial strains, plasmid construction, and gene knockout

B. atropi expressing tdTomato was created by mini-Tn7 tagging as describe before and the site of insertion was confirmed by arbitrary PCR and Sanger sequencing[38].

In-frame deletion was carried out as described previously[39]. Briefly, 1.5-kb fragments upstream and downstream of genes of interest (including the first and last 5-10 codons, respectively) were cloned and performed Gibson assembly together with the triple-digested vector pCVD443 (NEBuilder HiFi DNA Assembly Cloning Kit E5520S, New England BioLabs Inc.). Assembly mixture was then used to transformed *E. coli* SM10 λpir by electroporation (MicroPulser Electroporator, Bio-Rad). The parental *E. coli* SM10 strain was used to mate with wild-type *B. atropi*. Exconjugants were selected for first recombination event with antibiotics and subsequently second recombination event with sucrose. Putative knockout colonies were confirmed for deletion of gene of interest by colony PCR with primers flanking the gene.

Complementation was performed by mating the filamentation mutant strain LUAb7 with *E. coli* SM10 that had been transformed with plasmid pANT4 constitutively expressing a wild-type copy of the gene *gtaB*.

In vitro filamentation assay

A single colony from a streaked plate was inoculated into an overnight culture for each bacterial strain. The overnight cultures (OD_{600} ~ 0.4-0.5) were diluted to OD_{600} ~ 0.2 with LB and 200 μL were used to seed 4.8 mL of either LB or TB media. Cultures were incubated at 32°C, 100 rpm. After 2 days, all cultures were blinded. Each blinded culture was resuspended gently by pipetting slowly with P1000 pipette once to avoid breaking filaments and 7 μL of the culture was mounted on glass slides for imaging with a fluorescent Nikon Ni-E Eclipse. For each condition, several random frames from the slide were taken and a total of 500 microbes or more were counted. These microbes could be either filaments (longer than 4 μm), elongated cells (less than 4 μm but longer than a typical coccobacillus), or coccobacilli (~0.5-1 μm). Only the filamentous microbes were counted toward the filament percentage, calculated using the ratio of the number of filamentous microbes to the total number of cells.

In vitro selection for filamentation mutants

Wild type *B. atropi* was subjected to filamentation induction by switching from LB to 5 mL of TB plus 200 μg/mL cefotaxime and grown at 32°C, 100 rpm for 2 days. Cultures were syringe filtered through a 5.0 μm PVDF membrane (Millex SV) with gentle, slow pressing and 200 ml of the flowthrough was used to seed 4.8 mL of TB plus cefotaxime for another cycle of induction. Between each selection cycle, cultures were analyzed post-filamentation induction by gently resuspending with P1000 pipette once and mounting 3 x 7 ml to determine the filament percentage as described above. If greater than 5% of the population filamented, then the culture went through another round of selection. If less than 5% filamented, the flowthrough was plated on LB to isolate single colonies. Select colonies were tested for in vitro filamentation in TB, leading to the isolation of LUAb4.

In vitro bacterial growth curve

Overnight cultures of either WT or LUAb7 were diluted to OD_{600} ~ 0.2 with LB. Each of the diluted cultures was added to 12 wells (total of 36) of a clear bottom, non-cell culture treated 96-well plate. The peripheral wells were added with sterile DI water to minimize evaporation during OD_{600} reading. OD_{600} values were taken at 1 hour interval for 36 hours at 32°C using tunable Versa max microplate reader (software SoftMax Pro 6.3) with settings for 30-second shaking before actual reading of the OD_{600}. The final OD values at each time point for each condition was averaged from the 12 readings subtracted by the average blank reading (LB).

Intestinal cell-to-cell spreading assay

JU1501 was grown on OP50-1 food source and collected into a 15 mL centrifuge tube with M9T. Large animals (L3s, L4s, and adults) were allowed to settle to the bottom of the tube and the liquid on top containing mainly L1s and L2s was transferred to another 15 mL centrifuge tube. L1 and L2 animals were pelleted by centrifuging at 3000 x g for 1 minute and the animal pellets were divided into three parts and used for the standard pulse infection procedure as described above. After 2-hour pulse infection, animals were washed with MTEG buffer (M9T buffer, 0.25

mM EDTA, 10 µg/mL gentamycin) to kill extracellular bacteria. At 34 hpi, animals were collected for FISH.

FISH samples were scanned from the top right corner to the left, bidirectionally, to look for animals with distinguishable infection events. Each contiguous infection event is expected to result from a single cellular invasion, with a bacterium either filamenting or undergoing binary division resulting in a cluster of replicating coccobacilli. A total of 15 animals were imaged per condition, each containing between 1-10 distinguishable infection events. Images were taken with Zeiss LSM 710 inverted confocal microscope (software Zen 2012 SP1 Black edition, Zeiss LSM 710 release version 8.1.0.0) in z-stacks and analyzed with Fiji image software (version 2.1.0/1.53h) to count the number of whole intestinal nuclei that are fully passed by a single infection event along the A-P axis.

Normalized anterior-posterior (A-P) infection length

Animals were grown on OP50-1 food source and infected with standard pulse infection procedure (see above). At 34 hpi, animals fixed for FISH. Each condition was then imaged randomly for at least 30 animals with a fluorescent Nikon Ni-E Eclipse. Images were analyzed for normalized A-P infection length with Fiji image software (version 2.1.0/1.53h). In brief, for each animal in a particular condition, the distance between the most anterior and the most posterior points of a distinct, contiguous infection area was measured. If an animal had more than one contiguous infection area, the distances were averaged. This averaged A-P length of contiguous infection areas was then normalized to the length of the same infected animal to give the normalized A-P infection length.

Membrane dye and phalloidin staining of *O. tipulae*

Animal fixation and cuticle reduction were adapted from[40]. Worms were fixed with pre-chilled 4% paraformaldehyde in PBS at room temperature on a rotator for 30 minutes and moved to 4°C overnight. Animals were then washed 3 times with reduced cuticle buffer before incubating with fresh reduced cuticle buffer at 4°C for 24 hours. Afterwards, reduced animals were treated with 0.5 kU/mL collagenase type VII (C0773, Sigma Aldrich) at 37°C for ~32 hours. Afterwards, animals were rinsed once with DI water, followed by 3 washes with PBS, and store in PBS at 4°C for 1 day before staining. Animals were stained first with 0.5 mg/mL DAPI overnight. Excess DAPI was removed before staining with respective dyes. For membranes with a mixture of CellBrite Cytoplasmic membrane dye (Biotum) and BODIPY FL C_5-Ceramide (Invitrogen) at 400- and 1000-fold dilution, respectively, for 2 days. For phalloidin staining, Alexa 488-tagged phalloidin (ThermoFisher, 400x stock) was added at 4x working concentration and incubated for 2 days. All the staining was carried out in a thermal shaker at 37°C, 900 rpm.

CFSE dye staining of *O. tipulae*

Animals were infected with the pulse-chase procedure as described above. After 2 hours of infection, animals were washed twice with MTEG buffer then wash once with M9T buffer. Animals were then pelleted down by spinning at 0.4x g for 30 seconds. 500 µL of CFSE staining buffer (M9, 2.5 mM serotonin, 40 µg/mL CFSE

dye) was added and incubated for 3 hours. Animals were then plated on 6-cm NGM plate seeded with OP50 and another 500 µL of CFSE staining buffer was laid on top of the plate until animals were collected for FISH at 34 hpi.

Single nucleotide variation (SNV) calling

Strain LUAb7 was sequenced as described above using Illumina MiSeq. Reads were processed with cutadapt (v2.3) with parameters -u 10 -u -10 -U 10 -U 10 -m 50 to trim 10 bp from each end of every read and remove reads less than 50 bp[41]. Reads were mapped using bwa (v0.7.17-r1188) using the MarkDuplicates parameter[42]. SNVs were called using freebayes (v1.3.2-dirty) with parameter -C 50 requiring at least 50 supporting observations, a minimum mapping quality of 20, and base quality of 30[43], with the resulting data annotated by hand to look for SNVs with >90% of reads containing the variation. Raw reads from LUAb7 sequencing are available at Sequence Reads Archive (SRA) accession SRR14751734.

DATA AVAILABILITY

This Whole Genome Shotgun project for *B. atropi* type strain LUAb4 has been deposited at DDBJ/ENA/GenBank under the accession XXXXXX. The version described in this paper is version XXXXXX. Raw reads from LUAb7 sequencing are available at Sequence Reads Archive (SRA) accession XXXXX. All data supporting this manuscript are available from the corresponding author upon request.

REFERENCES

1. Colonne, P. M., Winchell, C. G. & Voth, D. E. Hijacking host cell highways: Manipulation of the host actin cytoskeleton by obligate intracellular bacterial pathogens. *Front. Cell. Infect. Microbiol.* **6**, 107 (2016).
2. Weddle, E. & Agaisse, H. Principles of intracellular bacterial pathogen spread from cell to cell. *PLoS Pathog.* **14**, e1007380 (2018).
3. Kespichayawattana, W., Rattanachetkul, S., Wanun, T., Utaisincharoen, P. & Sirisinha, S. *Burkholderia pseudomallei* induces cell fusion and actin-associated membrane protrusion: A possible mechanism for cell-to-cell spreading. *Infect. Immun.* **68**, 5377–5384 (2000).
4. Dunphy, P. S., Luo, T. & McBride, J. W. *Ehrlichia* moonlighting effectors and interkingdom interactions with the mononuclear phagocyte. *Microbes Infect.* **15**, 1005–1016 (2013).
5. Nikitas, G. *et al.* Transcytosis of *Listeria monocytogenes* across the intestinal barrier upon specific targeting of goblet cell accessible E-cadherin. *J. Exp. Med.* **208**, 2263–2277 (2011).
6. Justice, S. S., Hunstad, D. A., Cegelski, L. & Hultgren, S. J. Morphological plasticity as a bacterial survival strategy. *Nat. Rev. Microbiol.* **6**, 162–8 (2008).
7. Yang, D., Blair, K. & Salama, N. Staying in Shape: the Impact of Cell Shape on Bacterial Survival in Diverse Environments. *Microbiol. Mol. Biol. Rev.* **80**, 187–203 (2016).
8. Frirdich, E. & Gaynor, E. C. Peptidoglycan hydrolases, bacterial shape, and pathogenesis. *Curr. Opin. Microbiol.* **16**, 767–778 (2013).
9. Dalle, F. *et al.* Cellular interactions of *Candida albicans* with human oral epithelial cells and enterocytes. *Cell. Microbiol.* **12**, 248–271 (2010).

10. Tecle, E. *et al.* The purine nucleoside phosphorylase pnp-1 regulates epithelial cell resistance to infection in C. elegans. *PLoS Pathog.* **17**, e1009350 (2021).
11. Willis, A. R. *et al.* A parental transcriptional response to microsporidia infection induces inherited immunity in offspring. *Sci. Adv.* **7**, eabf3114 (2021).
12. Kim, D. H. & Ewbank, J. J. Signaling in the innate immune response. in *WormBook* 1–35 (2018). doi:10.1895/wormbook.1.83.2.
13. Balla, K. M., Luallen, R. J., Bakowski, M. A. & Troemel, E. R. Cell-to-cell spread of microsporidia causes *Caenorhabditis elegans* organs to form syncytia. *Nat. Microbiol.* **1**, 16144 (2016).
14. Osman, G. A. *et al.* Natural Infection of *C. elegans* by an Oomycete Reveals a New Pathogen-Specific Immune Response. *Curr. Biol.* **28**, 640-648.e5 (2018).
15. Panek, J. *et al.* A cullin-RING ubiquitin ligase promotes thermotolerance as part of the intracellular pathogen response in Caenorhabditis elegans. *PNAS* **117**, 7950–7960 (2020).
16. Schulenburg, H. & Félix, M. A. The natural biotic environment of Caenorhabditis elegans. *Genetics* **206**, 55–86 (2017).
17. Baïlle, D., Barrière, A. & Félix, M. A. *Oscheius tipulae*, a widespread hermaphroditic soil nematode, displays a higher genetic diversity and geographical structure than *Caenorhabditis elegans*. *Mol. Ecol.* **17**, 1523–1534 (2008).
18. Troemel, E. R., Félix, M.-A., Whiteman, N. K., Barrière, A. & Ausubel, F. M. Microsporidia are natural intracellular parasites of the nematode *Caenorhabditis elegans*. *PLoS Biol.* **6**, 2736–52 (2008).
19. Zhang, G. *et al.* A Large Collection of Novel Nematode-Infecting Microsporidia and Their Diverse Interactions with Caenorhabditis elegans and Other Related Nematodes. *PLoS Pathog.* **12**, e1006093 (2016).
20. Weiss, A. The Genus Bordetella. *Prokaryotes* 648–674 (2006).
21. Dichtel, M. L., Louvet-Vallée, S., Viney, M. E., Félix, M. A. & Sternberg, P. W. Control of vulval cell division number ha the nematode *Oscheius/Dolichorhabditis* sp. CEW1. *Genetics* **157**, 183–197 (2001).
22. Taylor-Mulneix, D. L. *et al. Bordetella bronchiseptica* exploits the complex life cycle of *Dictyostelium discoideum* as an amplifying transmission vector. *PLoS Biol.* **15**, 1–28 (2017).
23. Domingo, D. T., Jackwood, M. W. & Brown, T. P. Filamentous Forms of *Bordetella avium*: Culture Conditions and Pathogenicity. *Avian Dis.* **36**, 707–713 (1992).
24. Berbis, M., Sanchez-Puelles, J., Canada, F. & Jimenez-Barbero, J. Structure and Function of Prokaryotic UDP-Glucose Pyrophosphorylase, A Drug Target Candidate. *Curr. Med. Chem.* **22**, 1687–1697 (2015).
25. Wang, J. D. & Levin, P. A. Metabolism, cell growth and the bacterial cell cycle. *Nat. Rev. Microbiol.* **7**, 822–827 (2009).
26. Hill, N. S., Buske, P. J., Shi, Y. & Levin, P. A. A Moonlighting Enzyme Links *Escherichia coli* Cell Size with Central Metabolism. *PLoS Genet.* **9**, e1003663 (2013).
27. Weart, R. B. *et al.* A Metabolic Sensor Governing Cell Size in Bacteria. *Cell* **130**, 335–347 (2007).
28. Marolda, C. L. & Valvano, M. A. The GalF protein of Escherichia coli is not a UDP-glucose pyrophosphorylase but interacts with the GalU protein possibly

to regulate cellular levels of UDP-glucose. *Mol. Microbiol.* **22**, 827–840 (1996).
29. Rosen, D. A., Hooton, T. M., Stamm, W. E., Humphrey, P. A. & Hultgren, S. J. Detection of Intracellular Bacterial Communities in Human Urinary Tract Infection. *PLoS Med.* **4**, e329 (2007).
30. Justice, S. S., Hunstad, D. A., Seed, P. C. & Hultgren, S. J. Filamentation by *Escherichia coli* subverts innate defenses during urinary tract infection. *PNAS* **103**, 19884–19889 (2006).
31. Ponnusamy, D. & Clinkenbeard, K. D. *Yersinia pestis* intracellular parasitism of macrophages from hosts exhibiting high and low severity of plague. *PLoS One* **7**, e42211 (2012).
32. Martínez-Lorenzo, M. J., Méresse, S., De Chastellier, C. & Gorvel, J. P. Unusual intracellular trafficking of *Salmonella typhimurium* in human melanoma cells. *Cell. Microbiol.* **3**, 407–416 (2001).
33. Morgan, E., Longares, J.-F., Félix, M.-A. & Luallen, R. J. Selective cleaning of wild Caenorhabditis nematodes to enrich for intestinal microbiome bacteria. *J. Vis. Exp.* **174**, e62937 (2021).
34. Luallen, R. J. *et al.* Discovery of a Natural Microsporidian Pathogen with a Broad Tissue Tropism in *Caenorhabditis elegans*. *PLOS Pathog.* **12**, e1005724 (2016).
35. Prjibelski, A., Antipov, D., Meleshko, D., Lapidus, A. & Anton Korobeynikov. Using SPAdes De Novo Assembler. *Curr. Protoc. Bioinforma.* **70**, e102 (2020).
36. Seemann, T. Prokka: Rapid prokaryotic genome annotation. *Bioinformatics* **30**, 2068–2069 (2014).
37. Na, S. I. *et al.* UBCG: Up-to-date bacterial core gene set and pipeline for phylogenomic tree reconstruction. *J. Microbiol.* **56**, 281–285 (2018).
38. Lambertsen, L., Sternberg, C. & Molin, S. Mini-Tn7 transposons for site-specific tagging of bacteria with fluorescent proteins. *Environ. Microbiol.* **6**, 726–732 (2004).
39. Shikuma, N. J. *et al.* Marine Tubeworm Metamorphosis Induced by Arrays of Bacterial. *Science (80-.).* **343**, 529–533 (2014).
40. Yu, C. C. *et al.* Expansion microscopy of *C. elegans*. *Elife* **9**, e46249 (2020).
41. Martin, M. Cutadapt removes adapter sequences from high-throughput sequencing reads. *EMBnet.journal* **17**, 10–12 (2011).
42. Li, H. & Durbin, R. Fast and accurate short read alignment with Burrows-Wheeler transform. *Bioinformatics* **25**, 1754–1760 (2009).
43. Garrison, E. & Marth, G. Haplotype-based variant detection from short-read sequencing. *arXiv* 1–9 (2012).

ACKNOWLEDGEMENT

We would like to thank Prof. Aharon Oren for his expertise in prokaryotic nomenclature and assistance in naming *B. atropi*. Thank you to Dalaena Rivera for helping come up with the name *B. atropi*. We would like to thank Dr. Anca Segall and Dr. Nick Shikuma for providing bacterial plasmids, access to equipment, and assistance with bacterial genetics. Thank you to Dr. Aaron Reinke for editing the manuscript.

Funding: California State University, CSUPERB New Investigator Award and San Diego State University (SDSU) University Grants Program (UGP) award to RJL. MAF is an Investigator of the Centre National de la Recherche Scientifique, France. SDSU Rees-Stealy Research Fellowship (RSRF) and University Graduate Fellowship (UGF) award to TDT.

AUTHOR CONTRIBUTIONS

TDT, M-AF, RJL conceptualized the project. TDT, RJL designed the experiments. TDT, MAA, DL, RJL performed the experimental studies. TDT, RJL carried out data analysis and wrote of the manuscript.

COMPETING INTERESTS

Authors declare that they have no competing interests.

DISPLAY ITEMS

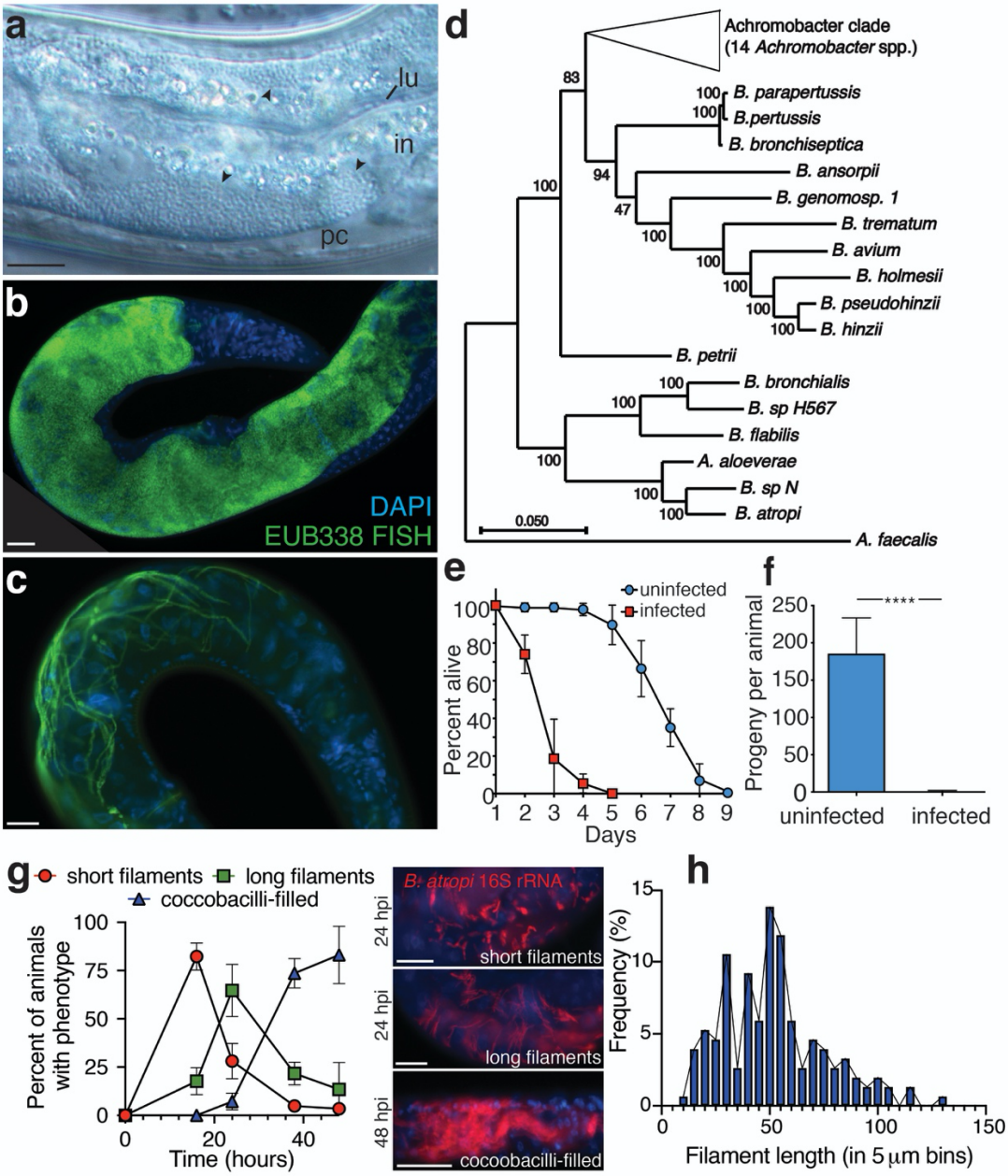

Figure 1. ***B. atropi* filaments in intestinal cells. a** A multitude of coccobacilli (*arrowheads*) inside the intestinal cells (*in*) of *O. tipulae* strain JU1501. The intestinal lumen (*lu*) and pseudocoelom (*pc*) are indicated. **b-c** FISH using a universal bacterial 16S rRNA probe EU338. Different animals shown from the same plate. Scale bars are 20 μm. **d** Phylogenomic tree of sequenced *Bordetella* and *Achromobacter* spp. with outgroup *Alcaligenes faecalis*. Branch lengths are the number of substitutions per site and branch points indicate percentage of trees with clustering of associated taxa. **e** Lifespan of JU1501 infected or uninfected with *B. atropi*, n=20 animals in 3 independent replicates. All graphs are presented with means and SD error bars. **f** Broodsizes of JU1501, **** is $p<0.0001$ by unpaired t test with Welch's correction, n=20 animals in 2 independent replicates. **g** Pulse chase infection time course of two independent replicates shown. Representative infection phenotypes are shown. Scale bars are 20 μm. **h** Histogram of in vivo filament lengths at 34 hpi.

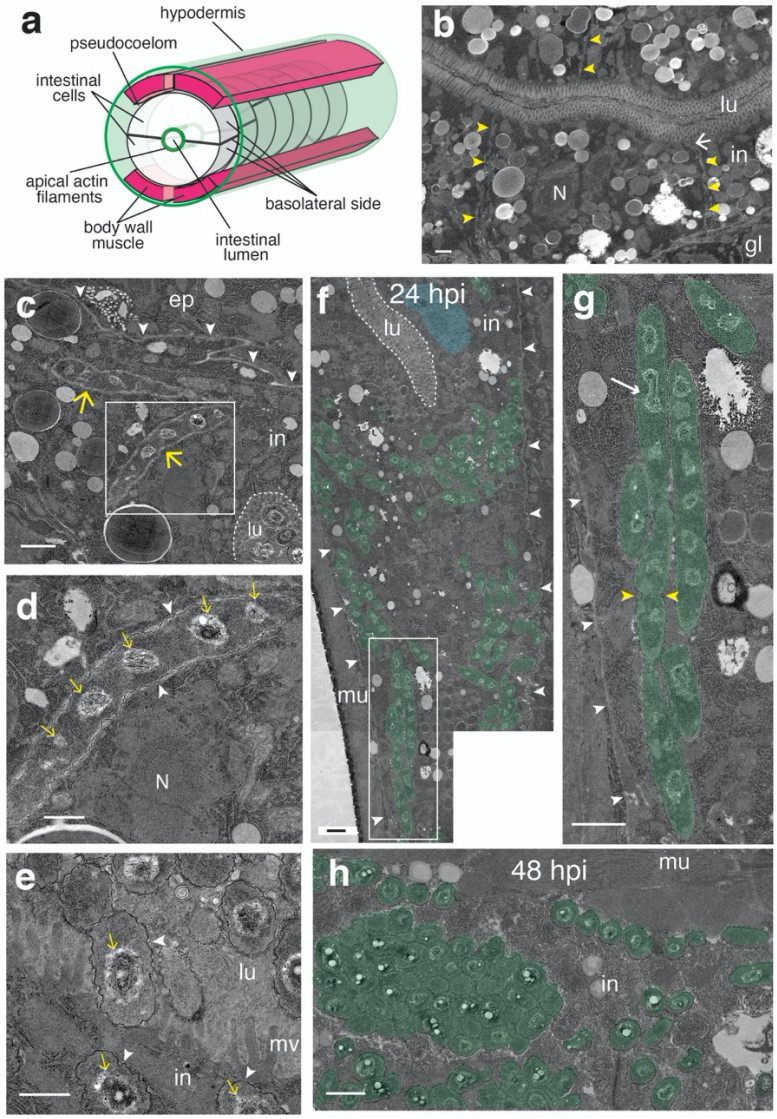

Figure 2. ***B. atropi* infects and forms filaments inside intestinal cells of *O. tipulae***. **a** A schematic of relative positions of intestine and surrounding tissues and compartments (not to scale, germline not shown for simplicity). **b** TEM of intestine of uninfected animals showing almost perpendicular cell-cell membranes delineation (yellow arrowheads), intestinal cell nucleus (N), and electron dense apical junctions (white arrows). Intestinal cells (in), lumen (lu), and germline (gl) are indicated. **c** *B. atropi* filaments (yellow arrows) in intestinal cells at 24 hpi. The pseudocoelom (yellow arrowheads), intestinal lumen (dashed line), and epidermis (ep) are indicated. **d** Inset of white box in **c** with electron-dense cell wall (arrowheads) outlining the filament containing multiple nucleoids (yellow arrows). The intestinal nucleus (N) is indicated. **e** Coccobacilli in the intestinal cytoplasm (in) and lumen (lu) have the same electron-dense cell wall and large nucleoids as filaments. Microvilli (mv) are indicated. **f** A micrograph of an infected animal at 24 hpi with *B. atropi* coccobacilli and filaments (pseudocolored green) in the intestine with the intestinal nucleus (pseudocolored blue), pseudocoelom (arrowheads), and body wall muscle (mu) indicated. **g** Inset of white-boxed region in **f** with potential dividing nucleoids and septum indicated by arrow and yellow arrowheads, respectively. **h** A multitude of coccobacilli in infected intestine at 48 hpi. Scale bars are 1 μm in **b**, **c**, **f**, **g**, **h** and 0.5 μm in **d** and **e**.

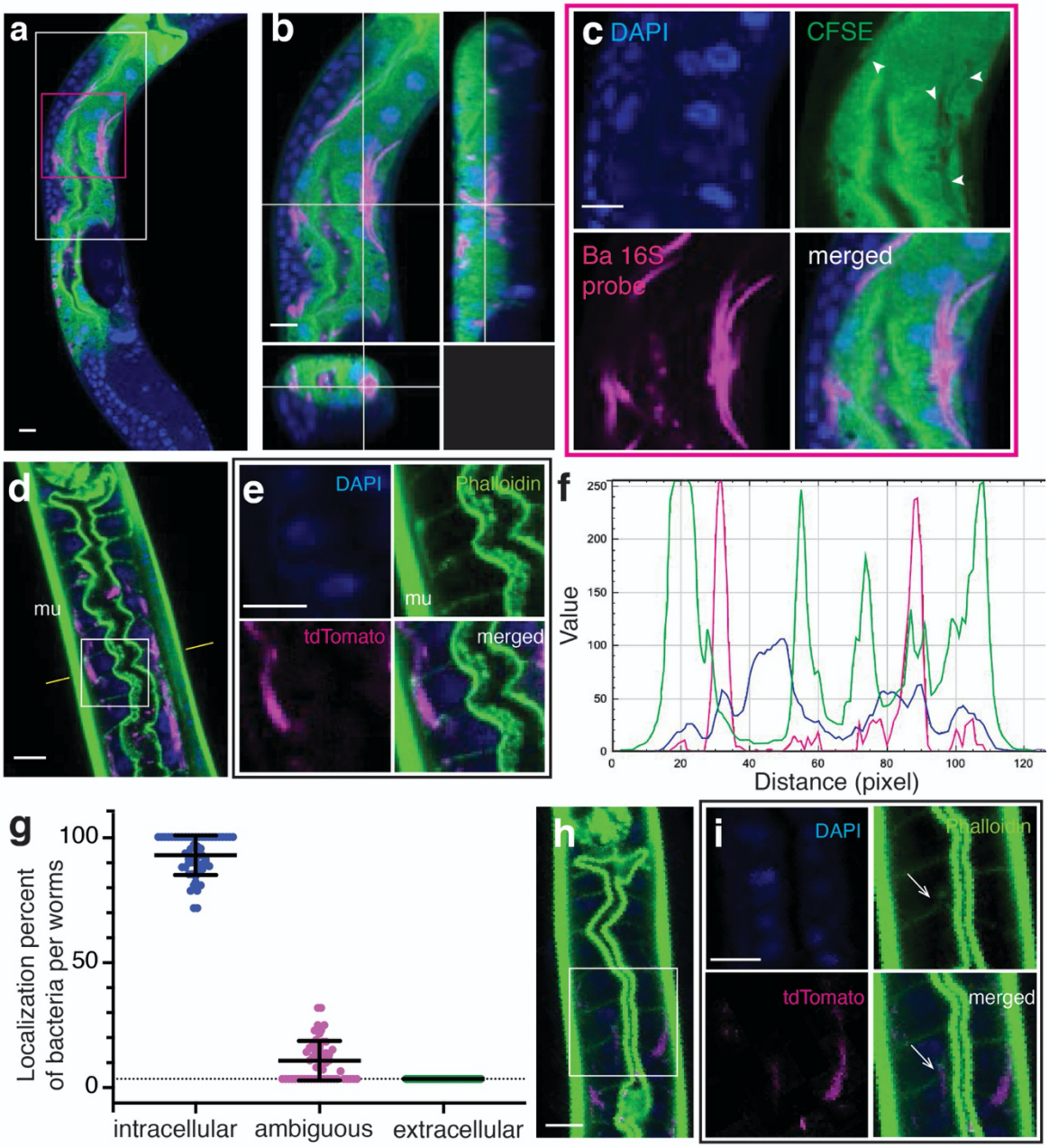

Figure 3. ***B. atropi* filaments localize with intestinal intracellular staining**. **a** Representative confocal image of FISH-stained animals infected with *B. atropi* and stained with the cytoplasmic dye, CFSE, which strongly stains the intestinal cell cytoplasm. **b** Orthogonal view of white-boxed region in **a**. **c** Higher magnification of red-boxed region in **a** showing CFSE-cleared areas (white arrowheads) are overlapped by signals from 16S probe specific-FISH to *B. atropi*. **d** Representative image of animals stained with phalloidin. **e** Higher magnification of region indicated by white box in **d** showing *B. atropi* presence in intestinal cells outlined by basolateral and apical actin filaments (mu, body wall muscle is indicated)**. f** Line profile analysis at the plane indicated by yellow lines in **d** showing localization of tdTomato (*B. atropi)* in between Alexa488-phalloidin (actin). **g** Quantification of localization of bacteria from **d**, n= 60 animals, N > 450 infection events in 2 independent replicates. **h** A phalloidin-stained animals with a fragment of filament pushing through intestinal lateral actin. **i** Inset indicated in **h.** Scale bars are 10 μm in **a-d** and **h**, and 5 μm in **e** and **i**.

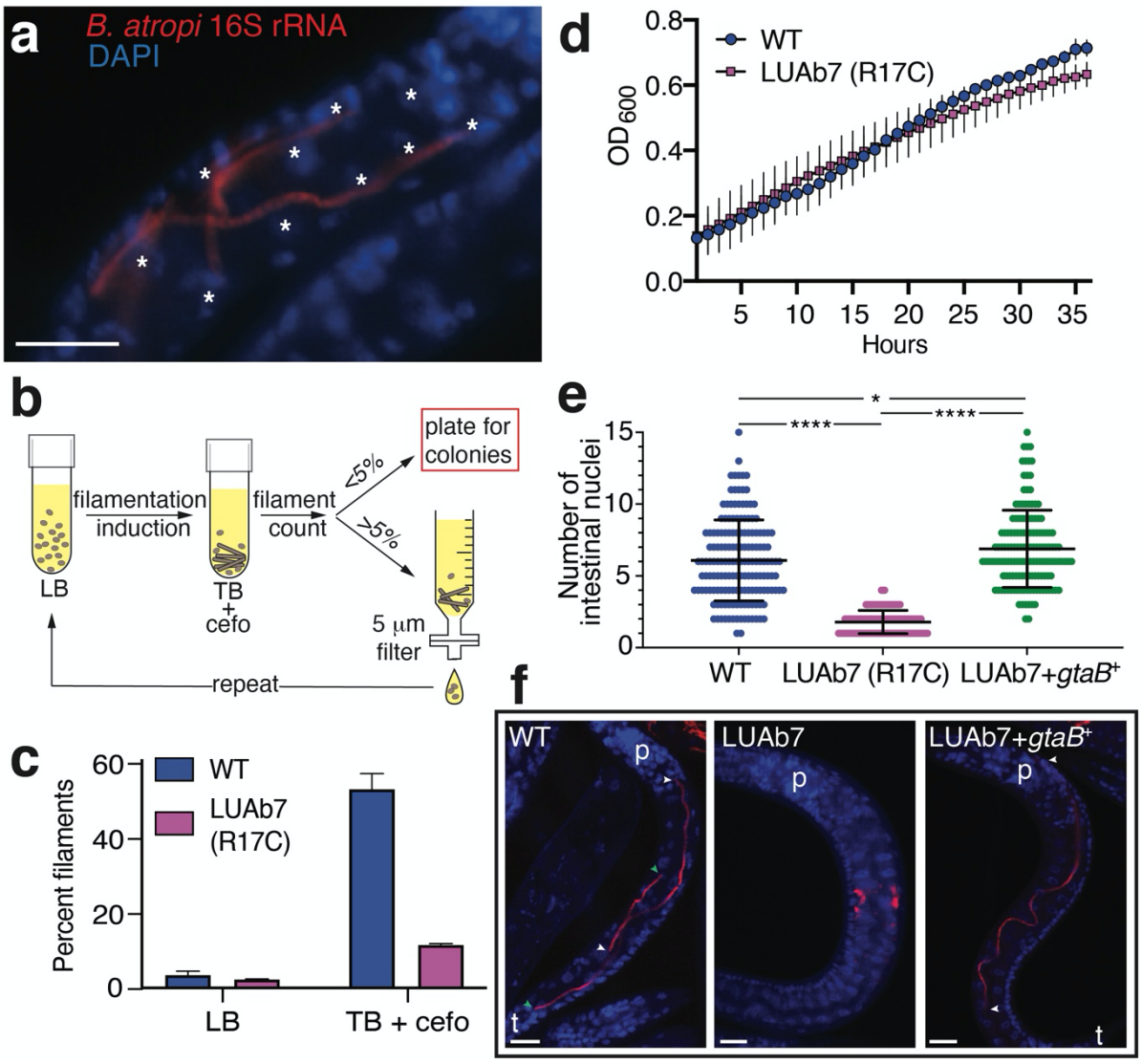

Figure 4. ***B. atropi* filaments invade multiple intestinal cells. a** Filaments of *B. atropi* in a larval *O. tipulae* animal with host nuclei indicated (*). **b** Schematic for selection of filamentation mutants. Filamentation was induced with TB + cefotaxime and counted for percent population with filaments, with >5% resulting in filtration followed by a repeat of induction and <5% resulting in plating to isolate single colonies. **c** Growth of *B. atropi* in LB or TB + cefotaxime, with percent filaments counted after 48 hours at 32°C. Bar graphs and plots are presented with means and SD error bars. **d** *B. atropi* strains grown in LB at 32°C for 36 hours with OD_{600} taken every hour. **e** Quantification of *B. atropi* infection in vivo by the number of intestinal nuclei that a single filament or contiguous infection passes along on the anterior-posterior axis. Results are from 2 independent replicates, n>60 infectious events per replicate, p<0.0001 (****) or p=0.014 (*) by Mann-Whitney two-tail t test. **f** Representative images from **e**, with filament ends (*color-matched arrowheads*), the pharynx (*p*) and tail (*t*) indicated. Scale bars are 10 µm.

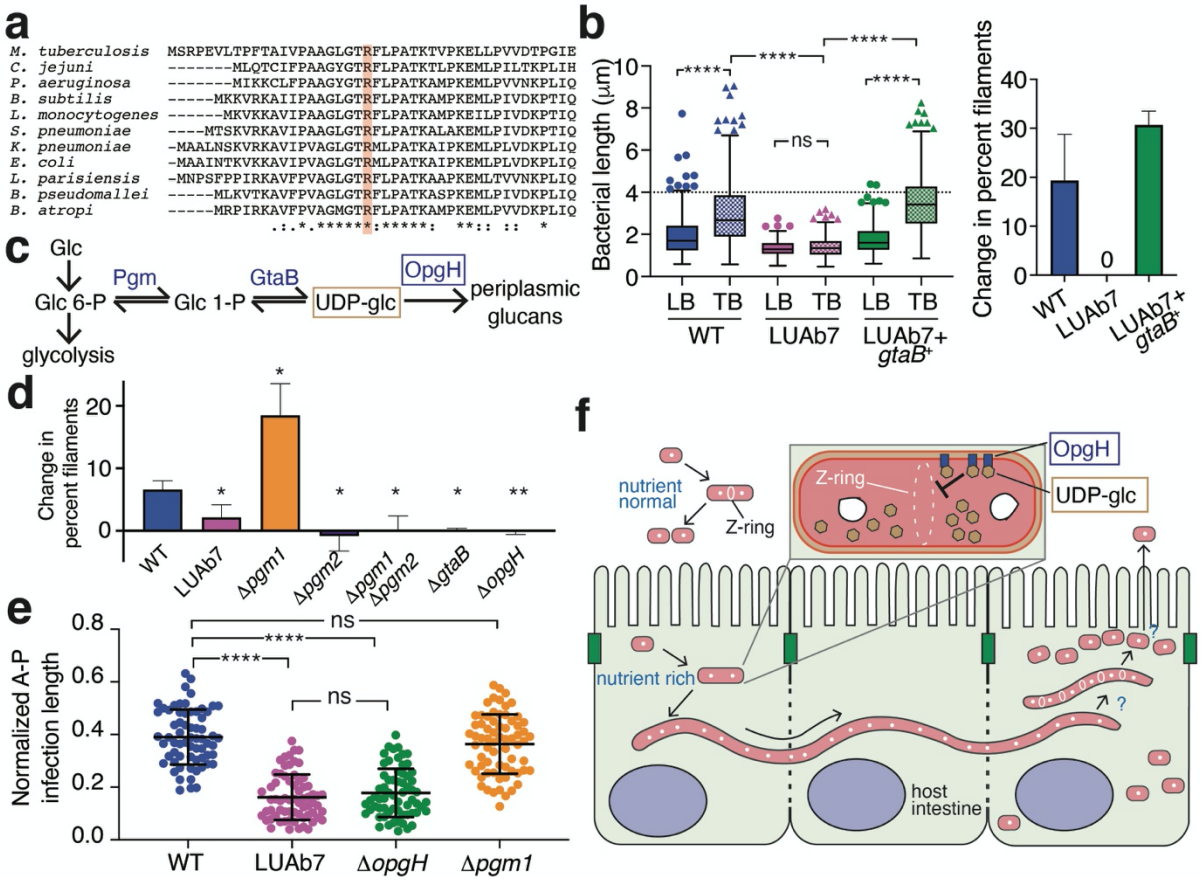

Figure 5. **The role of the UDP-glucose biosynthetic pathway in filamentation. a** CLUSTAL O multiple sequence alignment of GtaB from divergent bacteria with the predicted catalytic arginine highlighted. **b** In vitro filamentation of LUAb7(*gtaB*^{R17C}) and the complemented LUAb7 + *gtaB*$^{+}$ as measured by bacterial length in LB and TB (n=150, 2 independent replicates, Tukey's plot). The cutoff for a filament is 4 μm (hatched line) (*left*). The change in percent filaments was measured (% filaments in TB - % filaments in LB) (*right*). Scatter plots and bar graphs are presented with means and SD error bars. **c** The UDP-glucose biosynthetic pathway converting glucose (*glc*) to UDP-glucose (*UDP-glc*). **d** *B. atropi* knockouts measured for the change in percent filaments. Results are from 3 independent replicates, n>400 bacteria per replicate, p<0.05(*) or p<0.01(**) by unpaired two-tail t test with Welch's correction compared to WT. **e** Anterior to posterior (A-P) spreading of *B. atropi* mutants in vivo, normalized to animal length. Results are from 2 independent replicates, n=32-36 animals per replicate, p<0.0001 (****) or not significant (*ns*) by Mann-Whitney unpaired two-tail t test. **f** Model for *B. atropi* intracellular filamentation and spreading.